Int. J. Heat Mass Transfer. Vol. 29, No. 6, pp. 899–908, 1986
Printed in Great Britain

0017–9310/86 $3.00 + 0.00
Pergamon Journals Ltd.

Prediction of film cooling with a liquid coolant

T. R. SHEMBHARKAR and B. R. PAI
Propulsion Division, National Aeronautical Laboratory, Bangalore—560017, India

(*Received* 14 *May* 1985)

Abstract—A numerical method of analysing film cooling with a liquid coolant is presented. The model assumes a turbulent boundary-layer flow for the hot gas stream and a Couette flow in the liquid coolant film. A marching procedure is employed for solution of the equations of mass, momentum, enthalpy and species conservation. Numerical results for an air–water system are presented. The effects of flow conditions on the film cooling mechanism are discussed. An increase in free-stream temperature, free-stream velocity or coolant temperature causes reduction in the film-cooled length while an increase in coolant flow rate causes a proportionate increase in the film-cooled length. The comparison with the limited experimental data indicates that the observed trends are well predicted. However, more detailed data are required to validate and refine the prediction procedure particularly with regard to the flow within and on surface of the coolant film.

1. INTRODUCTION

FILM COOLING is an effective means of cooling a surface exposed to hot gases as in the case of gas turbine blades, combustors and rocket motors. Gaseous coolant is generally used in many of these applications. Several experimental and theoretical investigations have been carried out in gaseous film cooling. However, liquid coolant, having high heat absorbing capacity—including heat of vaporisation—has significant potential utility in high heat flux removal. One such application is film cooling of liquid rocket motors where a portion of liquid fuel is used as a coolant. Literature on liquid-film cooling is quite scanty compared to that on gaseous-film cooling. Experimental and theoretical investigations of liquid-film cooling of rocket motors have been conducted by Graham [1] and Sellers [2] who also reported some earlier investigations related to similar applications. The experiments of Graham and Sellers were conducted with a rocket motor burning liquid propellants at a combustion pressure of 345 kPa and at a thrust level of 2.2 kN. Kinney *et al.* [3] conducted experiments to determine the effectiveness of liquid-film cooling on the inner surface of horizontal tubes and studied the effect of parameters like temperature difference between the coolant and the hot air, air mass velocity, coolant flow rate and roughness of the tube surface. The theoretical models of Graham and Sellers were based on overall mass, momentum and energy balances. Their predictions do not take into consideration the details of transfer processes in the boundary layer. In the past, attempts have, however, been made to investigate the film-cooling process by boundary-layer analysis [4]. Recently there has been renewed interest in the related subjects of two-phase flow pertaining to evaporation. Chow and Chung [5] studied the evaporation of water into a laminar stream of hot air and superheated steam while Schröppel and Thiele [6] investigated liquid-film vaporisation in laminar and turbulent gas flows. Schröppel and Thiele solved the boundary-layer equations for the hot air stream assuming that the liquid film is at rest and the thickness of the film is constant.

The present investigation is aimed at developing a general numerical procedure for a two-dimensional film-cooling process in which the liquid coolant is injected tangentially along a surface exposed to a hot, turbulent gas stream. The liquid film thins down along the surface due to evaporation of liquid into the hot gas stream and also due to the shearing action of the hot gas. The entrainment of the liquid in the form of droplets into the gas stream, and the formation of waves on the liquid surface—which may be important for some cases—are not as yet accounted for in the present model. The framework of the method is quite general and could be extended to include these effects. The results presented here pertain to water as a coolant. The effects of various parameters like velocity and temperature of the hot gas and the coolant, on the evaporation process at the interface and the total film-cooled length are investigated.

2. PHYSICAL MODEL

A schematic diagram of the film-cooling process is shown in Fig. 1. Here, the surface which is exposed to a hot gas stream is protected by a liquid coolant film that is formed due to tangential injection of coolant along the surface. Heat is transferred from the hot gas to the coolant film and simultaneously mass transfer from the coolant film to the gas occurs as the coolant vaporises. The present objective is to solve the relevant conservation and thermodynamic equations in order to study the flow, heat and mass transfer details.

In a practical film-cooling situation, there will generally be complex, three-dimensional, turbulent flow in the vicinity of the coolant injection. Significant pressure gradients, radiative heat flux and combustion process may further complicate the flow. The liquid film may be turbulent and may become unstable due to

NOMENCLATURE

C_p specific heat
h enthalpy
H stagnation enthalpy
$\dot{J}_h$ enthalpy flux
$\dot{J}_m$ coolant mass flux
k thermal conductivity
K_p pressure gradient parameter, $(\nu/u^2 \cdot du/dx)_G$
l_m Prandtl mixing length
L latent heat of vaporisation
m mass concentration of coolant
$\dot{m}_c$ coolant flow rate
$\dot{m}_I''$ evaporation rate at interface
p partial pressure
P total static pressure
P_0 stagnation pressure
$\dot{q}_w$ wall heat flux
R gas constant
$\mathscr{R}$ universal gas constant
T temperature
T_0 stagnation temperature
u velocity in x-direction
v velocity in y-direction
W molecular weight
x distance along the wall
y distance perpendicular to the wall. For liquid film: y measured from the wall; for gas-side boundary layer: y measured from the interface
Δx step size
y_c coolant slot height.

Greek symbols
δ_G boundary-layer thickness
δ_C coolant film thickness
θ nondimensional temperature, $(T-T_I)/(T_G-T_I)$
λ, κ constants in mixing-length model
μ viscosity
ν kinematic viscosity
ρ density
σ_h Prandtl number
σ_m Schmidt number
τ shear stress.

Subscripts
a gas
c coolant
g gas and coolant vapour mixture
G free stream
I interface
t turbulent
v coolant vapour
w wall
eff effective
ref reference
sat saturation.

adverse flow conditions. Some portion of the liquid film may get entrained into the gas stream by formation of droplets. It is evidently quite a formidable task to simulate all these factors simultaneously. An attempt has, therefore, been made here to model the process with the following simplifying assumptions:

— the hot gas flow is a two-dimensional, turbulent, boundary-layer-type flow;
— the flow in the liquid film is a one-dimensional, laminar Couette flow;
— the surface of the film is smooth and the film remains stable all along the surface; and
— the gas mixture (hot gas + coolant vapour) exhibits a perfect gas law behaviour and is in equillibrium.

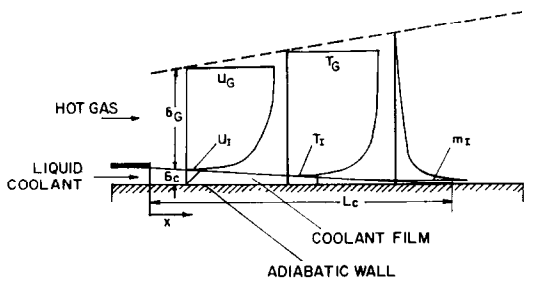

FIG. 1. Schematic diagram of liquid film cooling.

With these assumptions a Couette flow solution in the liquid film is matched to a two-dimensional, boundary-layer calculation for the gas side. The solution is marched in the flow direction satisfying the interface and other boundary conditions.

2.1. *Governing equations*

The one-dimensional, laminar Couette flow in the liquid film is described by the following equations:

Continuity

$$\frac{\partial u}{\partial x} = 0 \tag{1}$$

Momentum

$$\mu \frac{\partial^2 u}{\partial y^2} = \frac{dP}{dx} \tag{2}$$

Energy

$$\frac{\partial^2 T}{\partial y^2} = 0 \tag{3}$$

The two-dimensional, boundary-layer flow in the gas side is governed by the following conservation equations:

Continuity

$$\frac{\partial(\rho u)}{\partial x}+\frac{\partial(\rho v)}{\partial y}=0 \tag{4}$$

Momentum

$$\rho u\frac{\partial u}{\partial x}+\rho v\frac{\partial u}{\partial y}=\frac{\partial}{\partial y}\left[\mu_{\text{eff}}\frac{\partial u}{\partial y}\right]-\frac{\mathrm{d}P}{\mathrm{d}x} \tag{5}$$

Energy

$$\rho u\frac{\partial H}{\partial x}+\rho v\frac{\partial H}{\partial y}=\frac{\partial}{\partial y}\left[\frac{\mu_{\text{eff}}}{\sigma_{\text{h,eff}}}\frac{\partial H}{\partial y}\right]+\frac{\partial}{\partial y}\left[\mu_{\text{eff}}\left(1-\frac{1}{\sigma_{\text{h,eff}}}\right)\frac{\partial(u^2/2)}{\partial y}\right]+\frac{\partial}{\partial y}\left[\frac{\mu_{\text{eff}}}{\sigma_{\text{m,eff}}}\left(1-\frac{\sigma_{\text{m,eff}}}{\sigma_{\text{h,eff}}}\right)\times(h_{\text{v}}-h_{\text{a}})\frac{\partial m}{\partial y}\right] \tag{6}$$

Species concentration

$$\rho u\frac{\partial m}{\partial x}+\rho v\frac{\partial m}{\partial y}=\frac{\partial}{\partial y}\left[\frac{\mu_{\text{eff}}}{\sigma_{\text{m,eff}}}\frac{\partial m}{\partial y}\right]. \tag{7}$$

2.2. *Turbulence model*

The turbulent viscosity μ_{t} is estimated using the Prandtl mixing-length hypothesis:

$$\mu_{\text{t}}=\rho l_{\text{m}}^2\cdot|\mathrm{d}u/\mathrm{d}y| \tag{8}$$

where l_{m} is the Prandtl mixing length. A ramp distribution of l_{m} across the boundary layer is assumed [8], namely

$$\begin{aligned} l_{\text{m}}&=\kappa y, & 0<y<\lambda\delta_{\text{G}}/\kappa\\ l_{\text{m}}&=\lambda\delta_{\text{G}}, & \lambda\delta_{\text{G}}/\kappa<y<\delta_{\text{G}}. \end{aligned} \tag{9}$$

The effective viscosity, μ_{eff}, is obtained by the summation of the laminar and turbulent viscosities. The effective diffusion coefficients for enthalpy and mass transfer are estimated by the following relation

$$\frac{\mu_{\text{eff}}}{\sigma_{\text{eff}}}=\frac{\mu}{\sigma}+\frac{\mu_{\text{t}}}{\sigma_{\text{t}}} \tag{10}$$

where σ stands for Prandtl number (σ_{h}) or Schmidt number (σ_{m}). For the air–water system considered in this work, the following values have been used:

Prandtl numbers $\sigma_{\text{h}}=0.85,\quad \sigma_{\text{h,t}}=1.0$

Schmidt numbers $\sigma_{\text{m}}=0.6,\quad \sigma_{\text{m,t}}=1.0.$

2.3. *Interface conditions*

The solutions from the liquid side and the gas side must satisfy the following interface conditions:

Velocity

$$u_{\text{I}}=[u]_{\text{c,I}}=[u]_{\text{g,I}} \tag{11}$$

Temperature

$$T_{\text{I}}=[T]_{\text{c,I}}=[T]_{\text{g,I}} \tag{12}$$

Shear stress

$$\tau_{\text{I}}=[\mu(\partial u/\partial y)]_{\text{c,I}}=[\mu(\partial u/\partial y)]_{\text{g,I}} \tag{13}$$

Mass balance at the interface implying:

$$\dot{m}_{\text{I}}''=[-1/(1-m_{\text{I}})][\mu/\sigma_{\text{m}}(\partial m/\partial y)]_{\text{I}} \tag{14}$$

Heat balance at the interface implying:

$$-[k(\partial T/\partial y)]_{\text{c,I}}=-[k(\partial T/\partial y)]_{\text{g,I}}+\dot{m}_{\text{I}}''L. \tag{15}$$

3. SOLUTION PROCEDURE

3.1. *Couette flow solution*

The Couette flow equations (1)–(3) can be readily integrated to obtain the following velocity and temperature profiles in the liquid film:

$$u=\frac{1}{2\mu}\frac{\mathrm{d}P}{\mathrm{d}x}y^2+(\tau_{\text{w}}/\mu)y \tag{16}$$

$$T=(-\dot{q}_{\text{w}}/k)y+T_{\text{w}}. \tag{17}$$

The continuity equation can be integrated to obtain the variation of liquid film thickness δ_{c} along the surface. This integration yields:

$$\dot{m}_{\text{I}}''+\frac{\mathrm{d}}{\mathrm{d}x}\left[\int_0^{\delta_{\text{c}}}\rho u\,\mathrm{d}y\right]=0. \tag{18}$$

For $\mathrm{d}P/\mathrm{d}x\simeq 0$, the following simplified expression for δ_{c} can be derived

$$\delta_{\text{c}}=\left[\frac{\left\{\int_0^{\delta_{\text{c}}}\rho u\,\mathrm{d}y\right\}_{x-\Delta x}-\dot{m}_{\text{I}}''\Delta x}{(\frac{1}{2}\rho\tau_{\text{w}}/\mu)}\right]^{1/2}. \tag{19}$$

3.2. *Boundary-layer solution procedure*

The boundary-layer equations for mass, momentum, enthalpy and concentration, i.e. equations (4)–(7), form a set of coupled, parabolic differential equations. They have been solved by the finite-difference procedure of Patankar and Spalding [7]. Certain modifications were necessitated by the presence of strong coupling between interface concentration, temperature and evaporation rate. These modifications mainly relate to introduction of an inner iteration cycle for enthalpy and concentration equations so that the interface conditions are accurately satisfied. Before describing the interation cycle, it may be appropriate here to define some of the variables appearing in the calculations.

(a) *Enthalpy of the mixture.* The enthalpy of the mixture of hot gas and liquid vapour is calculated from:

$$h=mh_{\text{v}}+(1-m)h_{\text{a}} \tag{20}$$

in which the enthalpy of liquid vapour h_{v} and that of gas h_{a} are given by:

$$h_{\text{v}}=C_{\text{p,c}}(T_{\text{sat}}-T_{\text{ref}})+L+C_{\text{p,v}}(T-T_{\text{sat}})$$

and

$$h_a = C_{p,a}(T - T_{ref}) + h_{ref}. \quad (21)$$

In order to keep the gradient of mixture enthalpy independent of the reference temperature T_{ref}, the numerical value of T_{ref} and h_{ref} have been taken as zero. Thus h_v and h_a are given by:

$$h_v = C_{p,c}T_{sat} + L + C_{p,v}(T - T_{sat})$$

$$\text{and} \quad h_a = C_{p,a}T. \quad (22)$$

The stagnation enthalpy H is obtained by

$$H = h + \tfrac{1}{2}u^2. \quad (23)$$

(b) *Density of the mixture.* Under the assumption that the mixture of gas and liquid vapour behaves like a perfect gas, the density of the mixture is calculated by the following relation:

$$\rho = P \Big/ \left[\mathscr{R}T \left(\frac{m}{W_v} + \frac{1-m}{W_a} \right) \right]. \quad (24)$$

(c) *Viscosity of the mixture.* Viscosities of gas and liquid vapour are independently calculated using power law variation with temperature. The viscosity of mixture is then estimated using the following square root formula:

$$\mu = \left[\mu_v \frac{m}{\sqrt{W_v}} + \mu_a \frac{(1-m)}{\sqrt{W_a}} \right] \Big/ \left[\frac{m}{\sqrt{W_v}} + \frac{(1-m)}{\sqrt{W_a}} \right]. \quad (25)$$

(d) *Interface concentration,* m_I. The interface concentration is obtained from the knowledge of the interface temperature. The partial pressure corresponding to the interface temperature is obtained from the thermodynamic table for water and the following equation is employed to estimate m_I:

$$m_I = p_v \Big/ \left[\frac{R_v}{R_a} P - \left(\frac{R_v}{R_a} - 1 \right) p_v \right]. \quad (26)$$

(e) *Heat conduction at the interface.* The calculation procedure utilises the value of interface enthalpy flux $\dot{J}_h$ in forming the finite-difference coefficients for the enthalpy equation. In the presence of mass transfer, $\dot{J}_h$ includes enthalpy flux due to mass transfer also and it is related to the interface heat conduction $[-k\,\partial T/\partial y]_{g,I}$ in the following way

$$[-k\,\partial T/\partial y]_{g,I} = \dot{J}_h - \dot{J}_m(\sigma_{m,eff}/\sigma_{h,eff})(h_v - h_a). \quad (27)$$

3.2. *Initial and boundary conditions*

The initial profiles of velocity, temperature and coolant concentration have to be specified to start the calculations. A 1/7th power law was assumed for the temperature and velocity profiles within the gas-side boundary layer. A linear profile for coolant concentration with interface concentration corresponding to inlet coolant temperature was assumed. Further, the velocity and temperature profiles were adjusted near the interface region to satisfy the interface condition so that the marching procedure yields a stable solution. The initial conditions for the liquid film are more difficult to characterise, since it is important to allow for the adjustments that take place when the liquid first comes into contact with the gas. What is generally known in a problem is the coolant mass flow rate and the geometrical exit height of the slot. The flow in the region just downstream of the slot exit would be extremely complex should a region of recirculation be present and, depending on the velocity difference between the gas stream and liquid, an adjustment in shear stress between the two would take place. If the gas velocity is high (as in most rocket chamber applications) it is reasonable to assume that the liquid layer immediately thins down to a level to offer a matching shear stress at the interface equal to that offered by the gas layer. This assumption has been incorporated in the program. Of course if this shear is high enough, it may cause breaking away of a portion of the film in the form of droplets. This phenomenon is not considered at the present level of modelling, but can be included subsequently. The initial profiles for the coolant were taken as those corresponding to Couette flow solutions. At the outer edge of the gas-side boundary layer, the free-stream conditions, namely prescribed free-stream velocity, stagnation enthalpy and concentration are satisfied. The interface conditions constitute the boundary conditions for the inner edge of the gas-side boundary layer and also for the outer edge of the Couette flow solution for the coolant film. The no-slip condition and zero-heat-flux (adiabatic) condition on the wall constitute the boundary conditions for the inner edge of the coolant film.

3.3. *Marching procedure*

After specifying the initial profiles for the dependent variables u, H and m, the numerical solution is advanced forward step by step as follows:

1. The interface concentration m_I, the evaporation rate $\dot{m}_I''$ and the enthalpy flux $\dot{J}_h$ are assigned their upstream values.
2. The finite-difference coefficients for the enthalpy and concentration equations (6) and (7) are calculated. The resulting algebraic equations are solved to obtain new downstream enthalpy and concentration profiles.
3. A new value of evaporation rate $\dot{m}_I''$ is calculated using equation (14).
4. A new value of interface temperature is obtained from the current value of interface enthalpy using equations (20) and (12).
5. A new value of heat conduction at the interface $[-k\,\partial T/\partial y]_{g,I}$ is calculated by using equation (15).
6. A new value of interface enthalpy flux $\dot{J}_h$ is calculated using equation (27).
7. A new value of interface concentration is calculated by using equation (26). The partial pressure of coolant vapour p_v in this equation corresponds to the new interface temperature.

8. Steps 2–7 are repeated until no significant change in either m_I or $\dot{m}_I''$ occurs. These steps constitute the inner iteration cycle referred to earlier.
9. The remaining equation, namely the momentum equation (5) is then solved without any further iteration. The interface conditions (11) and (13) are also satisfied.
10. This completes the calculation at the current station. At the next station, steps 2–9 are repeated and thus solution is marched forward.

During the computations, it was found necessary to employ under-relaxation in estimating new values of variables at the interface (steps 3, 4 and 7) in order to obtain stable solutions. Further, in order to avoid premature interruption or excessively large number of inner iterations, a minimum of two and a maximum of five inner iterations were prescribed as the limits for the inner iteration cycle.

4. RESULTS AND DISCUSSION

Two sets of computations have been done: one with parametric variations for a hypothetical air–water system and another corresponding to an experimental investigation by Kinney *et al.* [3]. All computations have been done with 100 grid points across the boundary layer. Initially, tests were carried out to check that the integral quantities such as overall mass, momentum and enthalpy were in fact being conserved during the computations.

4.1. *Datum case*

As the literature on liquid film cooling is quite scanty, a hypothetical datum case has been selected in order to study the effect of free stream and coolant conditions on the effectiveness of the film cooling process. The parameters for this datum case are as follows

Free-stream stagnation temperature

$$T_{0,G} = 973 \text{ K}$$

Free-stream stagnation pressure

$$P_{0,G} = 200 \text{ kPa}$$

Free-stream velocity

$$u_G = 300 \text{ m s}^{-1}$$

Initial boundary-layer thickness

$$\delta_G = 12.5 \text{ mm}$$

Coolant temperature

$$T_c = 303 \text{ K}$$

Coolant flow rate

$$\dot{m}_c = 0.05 \text{ kg s}^{-1} \text{ m}^{-1}$$

Coolant slot height

$$y_c = 0.5 \text{ mm}$$

Pressure gradient parameter

$$K_p = 0$$

Wall heat flux (adiabatic wall)

$$\dot{q}_w = 0 \text{ W m}^{-2}.$$

Figure 2 shows the longitudinal variation of interface velocity u_I, interface temperature T_I and evaporation rate $\dot{m}_I''$ and coolant film thickness δ_c. It may be noted that the initial profiles for velocity, enthalpy and species concentration may not be perfectly compatible and hence certain oscillations near the inlet are observed in different variations shown in the figure. The interface velocity shows gradual decrease with the distance indicating that the retardation effect of the wall is stronger than the accelerating effect of the gas stream. The initial peak near the slot seen in the figure is caused by the shearing action of the incoming hot air stream. The interface temperature T_I tends towards a practically constant value after the initial adjustment. It approaches a value of around 352.5 K for the initial coolant temperature of 303 K in this case. As the interface temperature is nearly constant, the interface species concentration of water vapour also varies only marginally along the surface. However, as the diffusion of water vapour into the hot air decreases gradually, the interface evaporation rate $\dot{m}_I''$ decreases with the distance. The coolant film thickness decreases due to evaporation of water as well as due to the interfacial shear stress. The initial oscillation observed in this case is caused by initial adjustment of profiles near the slot. The thickness is initially reduced due to shearing action of the hot air stream. The film-cooled length L_c defined as the distance beyond which the film ceases to exist or over which 99.9% of inlet coolant mass flow has evaporated, is 34.35 cm in this case.

Figure 3 shows the velocity, temperature and species concentration profiles across the boundary layer at $x = 30$ cm from the inlet. These profiles have shapes typical of turbulent boundary layers.

4.2. *Parametric study*

Computations have been done to study the effects of the following parameters on the process of film cooling, namely:

(a) Free-stream stagnation temperature, $T_{0,G}$
(b) Free-stream velocity, u_G
(c) Coolant temperature, T_c
(d) Coolant mass flow rate, $\dot{m}_c$.

Solutions have been obtained by changing one parameter at a time from the datum value indicated in the previous section. Results of these computations for different cases have been compared in terms of interface temperature, interface concentration and film-cooled length. Figures 4–6 show these comparisons. It may be noted that the x-axis in these figures shows the value of a particular parameter as a fraction of the value of the same parameter in the datum case. For convenience,

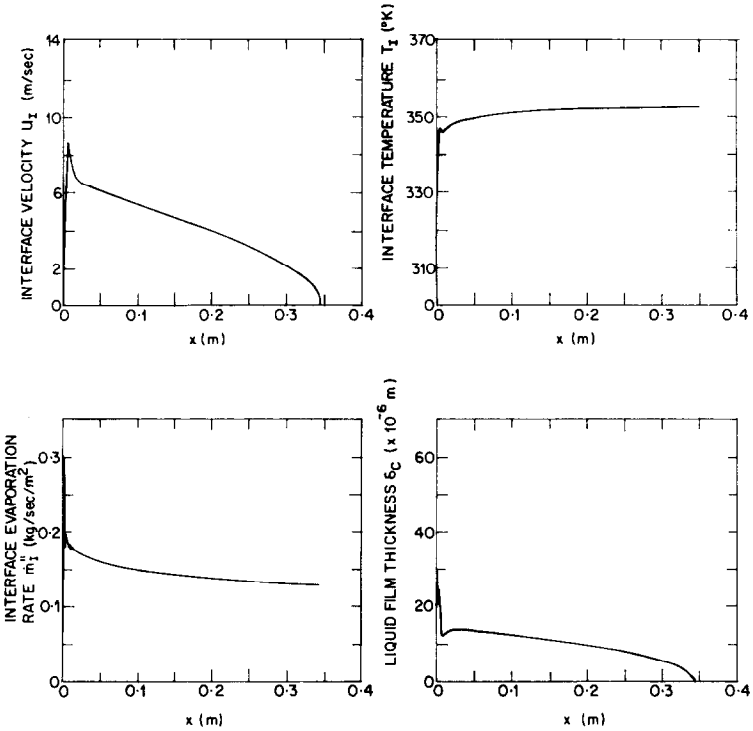

FIG. 2. Variation of interface velocity, temperature and evaporation rate, and liquid film thickness with distance for the datum case.

however, scales for variable parameters are also shown separately.

Figure 4 shows the variation of interface temperature T_I (at a fixed station, namely $x = 15$ cm) due to changes in different parameters. The free-stream temperature has a significant effect on the interface temperature which increases with increase in $T_{0,G}$. It is interesting to note that even for a free-stream stagnation temperature $T_{0,G}$ of 1973 K, the interface temperature (370 K) is well below the boiling point of the liquid coolant (391 K). The free-stream velocity also indicates noticeable change in T_I' which decreases as u_G is increased. The coolant temperature influences T_I in the same way as $T_{0,G}$. However, the coolant flow rate has essentially no influence on T_I. The interface temperature directly determines the partial pressure of water vapour p_v and thus influences the interface concentration m_I. The variation of m_I (at the same station $x = 15$ cm) for different cases is shown in Fig. 5. The free-stream temperature and coolant temperature have appreciable influence on m_I while the free-stream velocity and the coolant flow rate indicate no influence on m_I. It is interesting to note that the free-stream velocity, although influences T_I as shown in Fig. 4, shows no influence on m_I. This is due to the fact that these results have been obtained with a constant value of free-stream stagnation pressure $P_{0,G}$ which corresponds to different static pressure levels at different free stream velocities. The net effect of the two factors, namely the change in T_I and the change in static pressure level at different free stream velocities, is such that the interface concentration remains essentially constant as shown in Fig. 5.

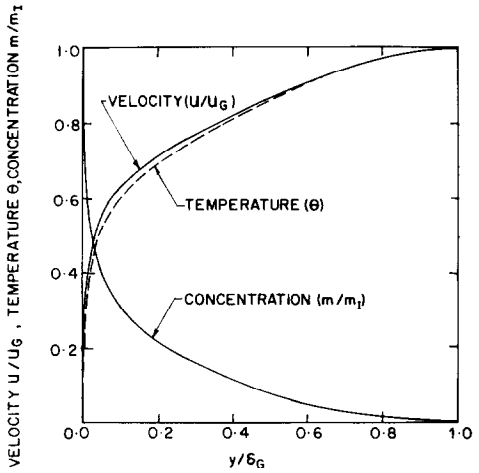

FIG. 3. Velocity, temperature and concentration profiles at X = 0.3 m for the datum case.

Figure 6 shows the effect of these parameters on the effectiveness of film cooling. The film-cooled length L_c may be taken as a measure of the effectiveness of film cooling. The figure shows the variation of L_c for different cases. The free-stream temperature and velocity have significant influence on L_c which decreases with increase of these parameters. The increase in $T_{0,G}$ causes increase in interface temperature and evaporation rate, and hence the film-cooled

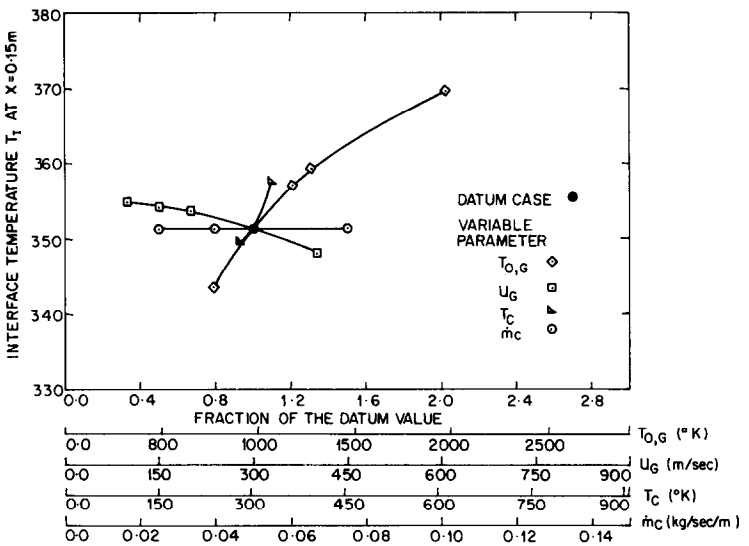

FIG. 4. Effect of different parameters on interface temperature.

length is significantly reduced. The increase in free-stream velocity, though causing no change in interface concentration, increases the evaporation rate due to increased diffusion of evaporated coolant vapour into hot air and thus reduces the film-cooled length. The higher coolant temperature reduces the film-cooled length due to increase in interface temperature causing higher evaporation rate. The coolant mass flow rate has negligible influence on interface temperature, concentration or evaporation rate. It does not influence the mechanism of the film-cooling process *per se*. The film-cooled length is therefore proportional to the coolant flow rate as shown in the figure.

Computations have also been done for accelerating flows by varying pressure gradient parameter K_p. In general, the effect of pressure gradient on film cooling is similar to that of free-stream velocity seen in Figs. 4–6. The film-cooled length decreases with increase in favourable pressure gradient. Interestingly, it is observed that the prediction of film-cooled length with pressure gradient is nearly equal to that with a constant free-stream velocity which is equal to local free-stream velocity at $x = L_c$ in the pressure gradient case.

4.3. *Comparison with experimental results of Kinney* et al. [3]

The experimental investigation of Kinney *et al.* [3] provides some data on liquid film cooling of internal surface of a horizontal tube. Though it is an internal flow situation, the present program which is based on boundary-layer analysis, has been used to predict their results. The flow conditions for a typical case have been

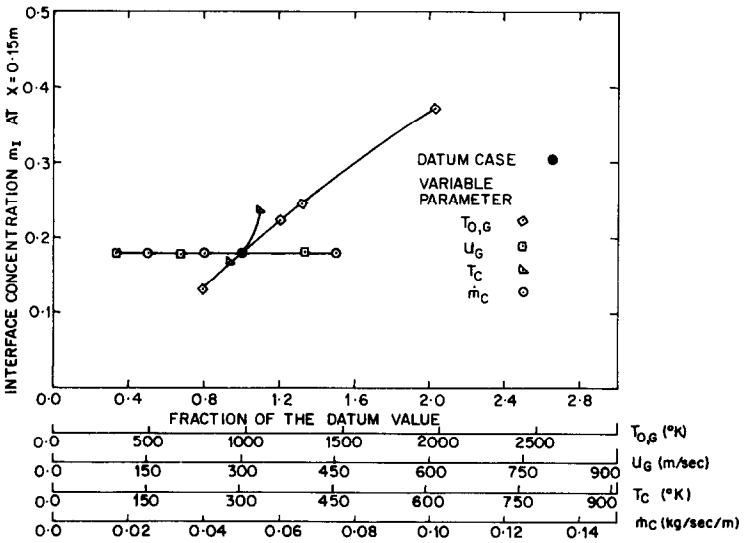

FIG. 5. Effect of different parameters on interface concentration.

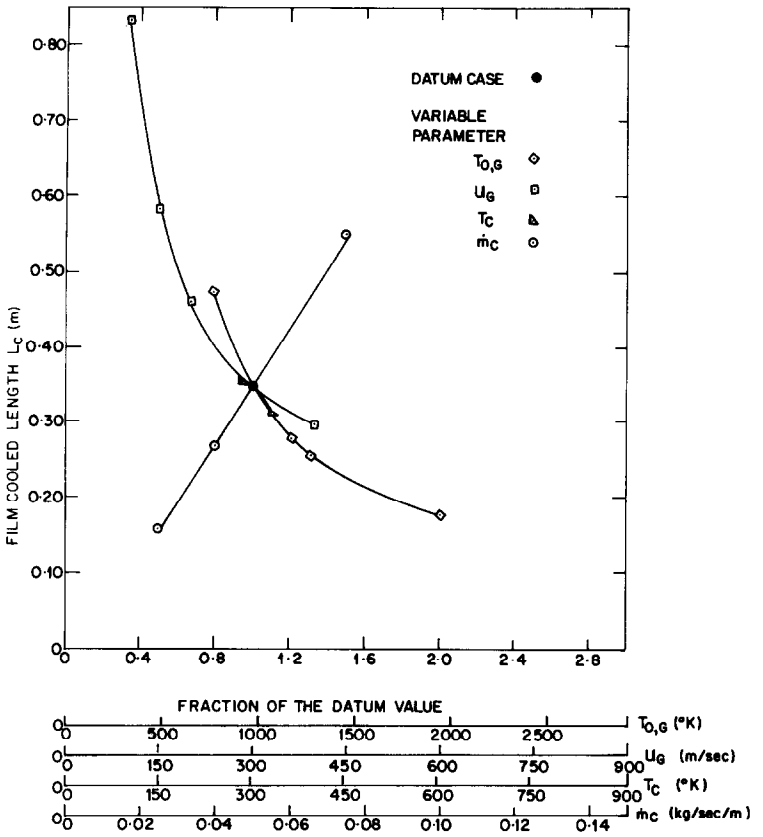

FIG. 6. Effect of different parameters on film-cooled length.

simulated as best as possible, based on the given information in ref. [3]. The conditions for the computations are:

Free-stream stagnation temperature

$$T_{0,G} = 1105 \text{ K}$$

Free-stream stagnation pressure

$$P_{0,G} = 214 \text{ kPa}$$

Free-stream velocity

$$u_G = 380 \text{ m s}^{-1}$$

Initial boundary-layer thickness (assumed)

$$\delta_G = 12.7 \text{ mm}$$

Coolant temperature

$$T_c = 303 \text{ K}$$

Coolant mass flow rate

$$\dot{m}_c = 0.0744\text{–}0.1274 \text{ kg s}^{-1} \text{ m}^{-1}$$

Coolant slot height

$$y_c = 0.584 \text{ mm}$$

Pressure gradient parameter

$$K_p = 0$$

Wall heat flux (adiabatic wall)

$$\dot{q}_w = 0 \text{ W m}^{-2}.$$

Figure 7 shows the variation of film-cooled length L_c with the coolant mass flow rate $\dot{m}_c$. The present predictions are compared with the results of Kinney *et al.* The experimental results indicate a linear variation of the film-cooled length with the coolant mass flow rate. The slope of the line, however, changes around $\dot{m}_c = 0.1 \text{ kg s}^{-1} \text{ m}^{-1}$. This is presumably caused by the onset of turbulent flow in the coolant film and the wavyness of the coolant film surface at high coolant flow rates. The present computations also predict linear variation of the film-cooled length with the coolant flow rate. The slope of the line also agrees very well with that observed in experiments at low coolant flow rates. However, the predictions are significantly higher than the experimental results and do not indicate the change of slope of the line at high coolant flow rates. The reasons for higher predictions are associated with lower values of interface temperature T_I in the predictions. It differs by about 10°C from the experimental value. As indicated above, the flow conditions employed in the boundary-layer predictions may not be matching perfectly with the conditions of the internal flow of the experiments. Further, the tube wall might have been getting heated by axial conduction in the experiments.

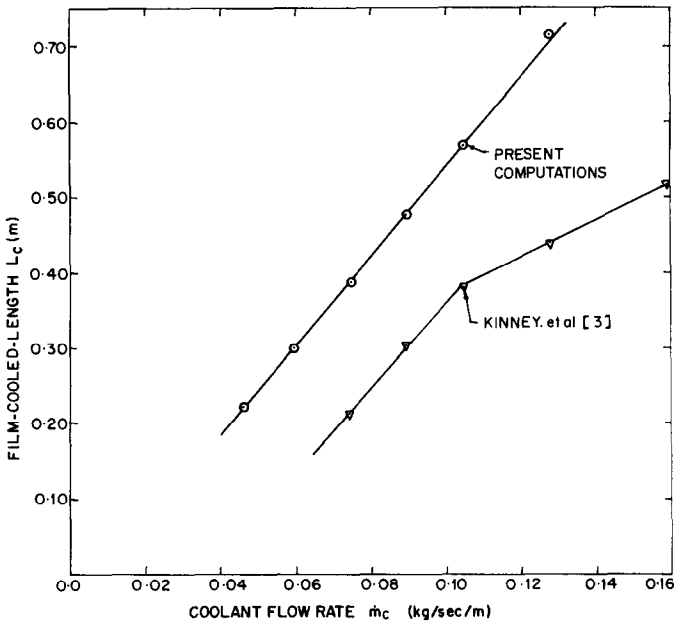

FIG. 7. Comparison of present computations with experimental results of Kinney *et al.* [3].

These factors may cause a higher interface temperature and increase the evaporation rate resulting in shorter film-cooled length in experiments. The change of slope in the experimental results at high coolant flow rates is not predicted by the present computations, which are based on the assumption that the coolant film is laminar, stable and smooth. Another difficulty in comparing film-cooled lengths is related to the precise point where the film vanishes. In the present calculations, as noted earlier, the film-cooled length has been taken as the distance from the slot over which 99.9% of the inlet coolant mass flow has evaporated. The computed value of the film thickness can approach small values—comparable to the height of surface texture elements of a typically machined surface. Thus for the predictions under consideration, if the film is assumed to vanish when it reaches a certain thickness, say 10 microns, a good agreement with the observed data can be projected. However, in view of the uncertainties mentioned above, it would be more appropriate to await more detailed data before the effect of surface roughness and other factors are incorporated in the prediction procedure.

5. CONCLUDING REMARKS

A numerical procedure has been used to model the film-cooling process with liquid coolant. Numerical results have been obtained for an air–water system. The effects of various parameters have been studied. The results indicate significant influence of free-stream temperature, free-stream velocity and coolant temperature on the heat and mass transfer at the interface. The procedure quantitatively predicts the increase in evaporation rate and resulting reduction in the film-cooled length due to increase in any of these parameters. An increase in coolant flow rate in the laminar-film regime does not influence the film-cooling mechanism as such and increases the film-cooled length proportionately. The discrepancies between the predictions and the experimental results of Kinney *et al.* suggest that the stability of the coolant film and the nature of the coolant film surface may have important influence on film cooling and they need to be modelled more realistically for better predictions.

REFERENCES

1. A. R. Graham, Film cooling of rocket motors. Ph.D thesis, Purdue University (1958).
2. J. P. Sellers, Jr, Experimental and theoretical study of the application of film cooling to a cylindrical rocket thrust chamber. Ph.D thesis, Purdue University (1958).
3. G. R. Kinney, A. E. Abramson and J. L. Sloop, Internal liquid film cooling experiments with air–stream temperature to 2000°F in 2- and 4-inch diameter horizontal tubes, NACA Report 1087, 1952.
4. H. W. Orth, DFVLR Report (in German), DLR FB 69-33 (1969).
5. L. C. Chow and J. N. Chung, Evaporation of water into a laminar stream of air and superheated steam, *Int. J. Heat Mass Transfer* **26**, 373–380 (1983).
6. J. Schröppel and F. Thiele, On the calculation of momentum heat and mass transfer in laminar and turbulent boundary layer flows along a vaporising liquid film, *Numer. Heat Transfer* **6**, 475–496 (1983).
7. S. V. Patankar and D. B. Spalding, *Heat and Mass Transfer in Boundary Layers*. Intertext, London (1970).

PREVISION DU REFROIDISSEMENT PAR FILM AVEC UN REFRIGERANT LIQUIDE

Résumé—On présente une méthode numérique pour analyser le refroidissement par film avec un réfrigérant liquide. Le modèle suppose un écoulement turbulent de couche limite pour le courant de gaz chaud et un écoulement de Couette dans le film liquide. Une procédure est utilisée pour la résolution des équations de conservation de masse, de quantité de mouvement, d'enthalpie et des espèces. Des résultats numériques pour un système air–eau sont présentés. Les effets des conditions d'écoulement sur le mécanisme de refroidissement par film, sont discutés. Un accroissement de la température de l'écoulement libre, de la vitesse de cet écoulement ou de la température du réfrigérant, cause une réduction de la longueur du film tandis qu'une augmentation du débit réfrigérant cause un accroissement proportionné de la longueur du film. La comparaison avec les données expérimentales peu nombreuses indique que les comportements observés sont correctement prédits. Néanmoins des données plus détaillées sont nécessaires pour valider et améliorer la procédure de calcul, particulièrement en ce qui concerne l'écoulement à l'intérieur et à la surface du film réfrigérant.

BERECHNUNG DER FILMKÜHLUNG MIT EINEM FLÜSSIGEN KÜHLMEDIUM

Zusammenfassung—Eine numerische Methode zur Analyse der Filmkühlung mit einem flüssigen Kühlmedium wird dargelegt. Im Modell wird eine turbulente Grenzschichtströmung für den heißen Gasstrom und eine Couette-Strömung im flüssigen Kühlfilm angenommen. Ein fortschreitendes Verfahren wird für die Lösung der Kontinuitäts-, Impuls-, Energie- und der Formerhaltungsgleichung angewendet. Die numerischen Ergebnisse für ein Luft–Wasser-System werden dargelegt. Die Auswirkungen der Strömungsbedingungen auf den Filmkühlmechanismus werden erörtert. Ein Anwachsen der Temperatur und Geschwindigkeit der ungestörten Gasströmung oder ein Ansteigen der Kühlmitteltemperatur bewirken eine Verringerung der filmgekühlten Länge; während ein Anwachsen des Kühlmittelmassenstroms ein proportionales Ansteigen der filmgekühlten Länge verursacht. Der Vergleich mit den wenigen zur Verfügung stehenden experimentellen Daten zeigt, daß die beobachteten Trends gut vorausberechnet werden. Es sind jedoch detailliertere Daten erforderlich, um das Vorhersageverfahren im Hinblick auf die Berücksichtigung der Strömung innerhalb und an der Oberfläche des Kühlmittelfilms zu bestätigen und zu verfeinern.

РАСЧЕТ ПЛЕНОЧНОГО ОХЛАЖДЕНИЯ

Аннотация—Предложен численный метод анализа пленочного охлаждения. Для потока горячего газа используется модель турбулентного пограничного слоя, а течение в пленке жидкого хладагента считается куэттовским. Для решения уравнений массы, импульса, энтальпии и сохранения полного количества данного компонента применяется метод прогонки. Представлены численные результаты для системы воздух–вода. Обсуждается влияние течения на механизм пленочного охлаждения. Рост температуры и скорости набегающего потока или температуры хладагента вызывает уменьшение длины участка пленочного охлаждения, в то время как увеличение скорости течения хладагента приводит к пропорциональному увеличению длины пленки. Сравнение численных результатов с имеющимися экспериментальными данными свидетельствует о хорошем их соответствии. Однако для обоснования и усовершенствования методики расчета, в частности, с учетом течения внутри и на поверхности пленки хладагента, требуются более тщательные исследования.